SNX9 Couples Actin Assembly to Phosphoinositide Signals and Is Required for Membrane Remodeling during Endocytosis

Defne Yarar,[1],* Clare M. Waterman-Storer,[1] and Sandra L. Schmid[1],*
[1] Department of Cell Biology, The Scripps Research Institute, La Jolla, CA 92037, USA
*Correspondence: yarar@scripps.edu (D.Y.), slschmid@scripps.edu (S.L.S.)
DOI 10.1016/j.devcel.2007.04.014

SUMMARY

Multiple modes of endocytosis require actin-dependent remodeling of the plasma membrane; however, neither the factors linking these processes nor their mechanisms of action are understood. The sorting nexin, SNX9, localizes to clathrin-coated pits where it interacts with dynamin and functions in clathrin-mediated endocytosis. Here, we demonstrate that SNX9 also localizes to actin-rich structures implicated in fluid-phase uptake, including tubular membranes containing GPI-anchored proteins and dorsal membrane ruffles. Moreover, we show that SNX9 is critical for dorsal ruffle formation and for clathrin-independent, actin-dependent fluid-phase endocytosis. In vitro, SNX9 directly associates with N-WASP, an Arp2/3 complex activator, and stimulates N-WASP/Arp2/3-mediated actin assembly. SNX9-stimulated actin polymerization is greatly enhanced by $PI_{4,5}P_2$-containing liposomes, due in part to $PI_{4,5}P_2$-induced SNX9 oligomerization. These results suggest a mechanism for the spatial and temporal regulation of N-WASP-dependent actin assembly and implicate SNX9 in directly coupling actin dynamics to membrane remodeling during multiple modes of endocytosis.

INTRODUCTION

Cells take up macromolecules and fluids through diverse endocytic pathways including macropinocytosis, clathrin-mediated endocytosis, caveolin-mediated endocytosis, and clathrin/caveolin-independent endocytosis (Conner and Schmid, 2003). Clathrin/caveolin-independent endocytosis encompasses several distinct, poorly characterized pathways (Kirkham and Parton, 2005). For example, a clathrin-independent endocytic pathway is induced upon dominant interference of dynamin GTPase activity, a key regulator of multiple endocytic pathways (Damke et al., 1995), whereas a clathrin-independent, dynamin- and RhoA-dependent endocytic pathway is used by the interleukin 2 receptor (Lamaze et al., 2001). In addition, recent studies have focused on a clathrin/caveolin-independent endocytic pathway used by GPI-anchored proteins (GPI-APs) that are internalized through tubular invaginations in the plasma membrane and traffic through a compartment called the GPI-AP-enriched early endosomal compartment (GEEC) (Kirkham and Parton, 2005; Mayor and Riezman, 2004; Sabharanjak et al., 2002).

Although clathrin-, caveolin-, and clathrin/caveolin-independent pathways are mechanistically distinct, many require the spatial and temporal coordination of F-actin assembly. Actin assembly plays a role in membrane remodeling events such as protrusion during macropinocytosis, invagination during clathrin- and caveolin-dependent endocytosis, and vesicle fission (Kaksonen et al., 2006; Merrifield et al., 2002, 2005; Pelkmans et al., 2002; Swanson and Watts, 1995; Yarar et al., 2005). However, little is known about the factors controlling the coordination of F-actin polymerization with membranes during these modes of endocytosis.

A small subset of endocytic accessory proteins has been implicated in functioning at the interface between membranes and the F-actin cytoskeleton. For example, Hip1R, Toca1, Cip4, and FBP17 contain phospholipid-binding domains and directly interact with components of the F-actin cytoskeleton (Engqvist-Goldstein et al., 1999; Ho et al., 2004; Itoh et al., 2005; Tsujita et al., 2006). However, it is unclear if any of these proteins utilize their lipid-binding properties to directly modulate F-actin dynamics. Thus, the proteins that directly convey signals from membranes to the regulation of F-actin dynamics for membrane remodeling during endocytosis remain to be defined.

We and others previously identified the sorting nexin, SNX9, as a major binding partner of dynamin (Lundmark and Carlsson, 2004; Soulet et al., 2005). SNX9 is essential for efficient clathrin-mediated endocytosis and is transiently recruited to clathrin-coated pits, along with dynamin, during late stages of vesicle formation (Soulet et al., 2005). The SNX family is defined by the phox homology (PX) domain, a phospholipid-binding module (Seet and Hong, 2006). SNX9 also contains an N-terminal SH3 domain that participates in protein-protein interactions and a BAR (Bin/amphiphysin/Rvs) domain, a second phospholipid-binding region that also functions in dimerization (Peter et al., 2004). SNX9 has been linked to the

F-actin cytoskeleton through an interaction with WASP (Worby et al., 2001; Badour et al., 2007), suggesting it may function in both endocytic and actin-related processes.

Here, we establish that SNX9 is required for clathrin-independent, actin-dependent fluid-phase endocytosis. SNX9 directly regulates F-actin nucleation through N-WASP and the Arp2/3 complex, and this activity is synergistically enhanced by $PI_{4,5}P_2$-containing liposomes. Our findings suggest a mechanism by which SNX9 physically couples F-actin nucleation to plasma membrane remodeling during endocytosis.

RESULTS

SNX9 Localizes with F-Actin-Rich Structures Implicated in Endocytosis

SNX9 transiently localizes to clathrin-coated pits on the plasma membrane, prior to vesicle formation (Lundmark and Carlsson, 2004; Soulet et al., 2005). However, in BSC1 epithelial cells expressing clathrin light chain-EGFP, we also observed surface-associated mCherry-SNX9 at sites other than those corresponding to coated pits, suggesting that it may associate with other endocytic sites. Therefore, to further investigate SNX9's function, we examined its subcellular localization by double labeling with other markers for endocytosis.

The GEEC pathway for internalization of GPI-APs has been reported to participate in the uptake of a large fraction of the fluid phase (Guha et al., 2003; Kirkham et al., 2005; Sabharanjak et al., 2002). Using time-lapse total internal reflection fluorescence microscopy (TIR-FM), we observed mCherry-SNX9 along the length of dynamic vesicular and tubular structures that were labeled with the model GPI-anchored protein, GFP-GPI. In addition, while we detected SNX9 foci devoid of GFP-GPI, we frequently observed bright mCherry-SNX9 foci transiently associated with the edges of these dynamic GFP-GPI tubules (Figure 1A and see Movie S1 in the Supplemental Data available with this article online).

Since SNX9 has been linked with WASP-family proteins (Worby et al., 2001; Badour et al., 2007), regulators of the actin cytoskeleton, we also analyzed the localization of the ubiquitously expressed vertebrate WASP-family protein, N-WASP, and of actin. Like mCherry-SNX9, mCherry-N-WASP localized along the length of GFP-GPI structures, as well as transiently at the edges of GFP-GPI structures (Figure 1B; Movie S2). We also observed flashes of mCherry-actin along the lengths of GFP-GPI tubules, often appearing brighter at the edges (Figure 1D; Movie S4). To determine if there was coordination between N-WASP with SNX9, we analyzed the relative localization of these two proteins and found that 80 ± 13% of mCherry-SNX9 foci (mean ± standard deviation, n = 118, four cells) transiently colocalized with a subset of EGFP-N-WASP foci (Figure 1C; Movie S3). Together, these data suggest that SNX9, N-WASP, and actin function in a spatially and temporally coordinated manner at sites of GPI-AP-containing membrane tubule formation.
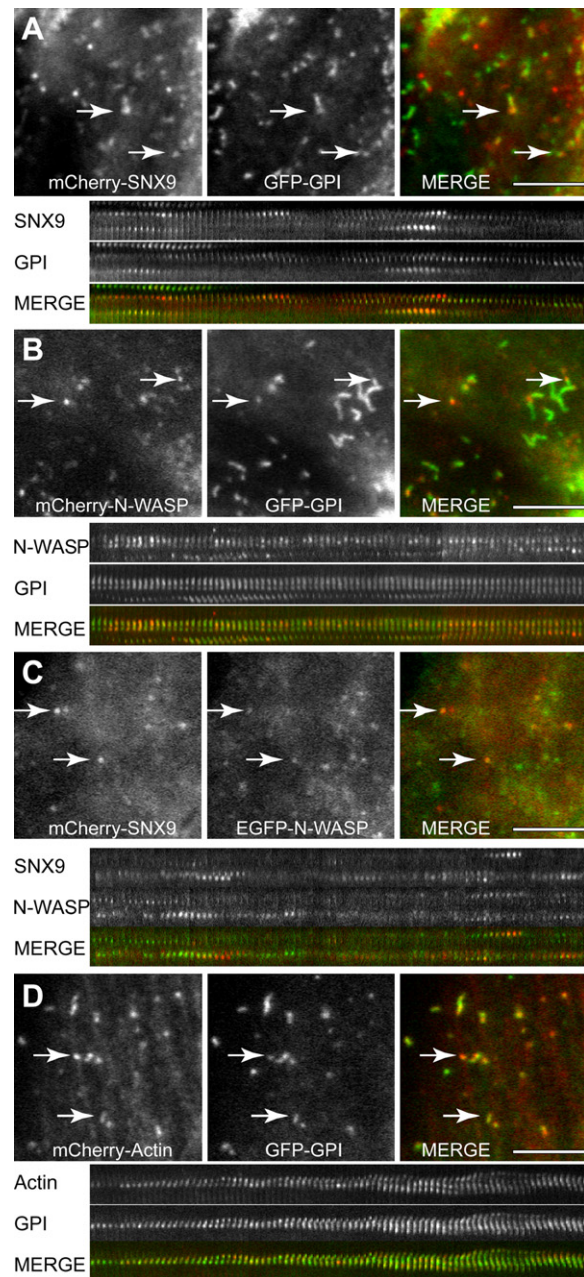
Figure 1. SNX9, N-WASP, and Actin Partially Colocalize with GPI-APs on the Plasma Membrane

(A, B, and D) SNX9 (A) N-WASP (B), and actin (D) each colocalize with GPI-APs on the plasma membrane, shown in regions of cells transiently expressing mCherry-SNX9 ([A], red in merge), mCherry-N-WASP ([B], red in merge), or mCherry-actin ([D], red in merge) and GFP-GPI ([A], [B], and [D], green in merge), and in kymographs of representative events. See Movie S1, S2, and S4.

(C) SNX9 and N-WASP are transiently colocalized at foci on the plasma membrane. Shown are regions of cells expressing mCherry-SNX9 (red in merge) and EGFP-N-WASP (green in merge) and representative kymographs. See Movie S3. Scale bars in cells = 5 µm. Scale bars in kymographs = 2 µm. Time scales of kymographs are (min:s) (A), 10:43; (B), 11:48; (C), 7:00; and (D), 10:48. See arrows for examples of overlapping structures.

We also detected punctate signals of SNX9 at circular dorsal rings and at a subset of membrane ruffles at the cell periphery in BSC1, Cos7, and Swiss 3T3 cells (Figure 2A; Figure S1A; data not shown). Structures similar to these have been implicated in fluid-phase endocytosis (Buccione et al., 2004; Suetsugu et al., 2003; Mettlen et al., 2006). Dorsal ruffles and rings are infrequent in normal cell populations but can be induced by treatment with PDGF (Buccione et al., 2004). Indeed, PDGF-induced dorsal ruffles and rings also contained SNX9 (Figure 2B; Figure S1A).

Previous studies have shown that dorsal ruffles and rings are rich in F-actin and in N-WASP (Buccione et al., 2004). Based on both fixed and live cell analyses, SNX9 partially colocalized with F-actin in these structures and could often be observed at the center of the dorsal rings (Figures 2A–2D; Figure S1). In living cells stimulated with PDGF, mCherry-SNX9 associated with punctate structures forming a ring at the dorsal surface (Figures 2C and 2D). A subset of these structures constricted over time, and mCherry-SNX9 was associated with tubulo-vesicular structures at the center of the constricted ring (Figure 2C; Movie S5). While EGFP-actin localization mostly paralleled that of mCherry-SNX9 in PDGF-induced dorsal rings, EGFP-actin was occasionally observed at the periphery (Figure 2D; Movies S6 and S7). In addition, mCherry-SNX9 and EGFP-N-WASP partially colocalized at dorsal rings following PDGF stimulation (Figure S2; Movie S8). Together, these results demonstrate that SNX9, NWASP, and actin are enriched at multiple F-actin-rich structures implicated in fluid-phase endocytosis.

Since SNX9 localized to F-actin-rich dorsal ruffles and rings, we tested whether it was required for the formation of these structures. Transfection of siRNAs targeting SNX9 resulted in depletion of greater than 90% of SNX9 protein but did not alter actin or dynamin levels (Figure 2E and data not shown). F-actin-rich dorsal ruffles and rings formed in 74 ± 12% (mean ± standard deviation) of control-depleted cells after PDGF stimulation (Figure 2F), whereas significantly fewer SNX9-depleted cells had dorsal ruffles and rings (12 ± 5%, p < 0.01; Figure 2F). These data demonstrate that, in addition to its known role in clathrin-mediated endocytosis, SNX9 is required for the efficient formation of PDGF-induced dorsal ruffles and rings on the plasma membrane.

SNX9 Is Required for Fluid-Phase Endocytosis

The GEEC pathway and peripheral and dorsal membrane ruffles have been implicated in endocytosis (Kirkham and Parton, 2005, Buccione et al., 2004; Suetsugu et al., 2003; Mettlen et al., 2006). Consistent with the dynamic association of SNX9 with these structures, a pronounced inhibition of fluid-phase endocytosis in SNX9-depleted cells relative to control siRNA-treated cells was observed as measured by the accumulation of Alexa-568-labeled dextran (Figure 3A). To quantify this effect, we measured horseradish peroxidase (HRP) uptake, a well-established fluid-phase marker (Figure S2A). Depletion of SNX9 resulted in a 59 ± 15% (n = 3, p = 0.004) reduction of con-

stitutive HRP internalization in comparison to control-depleted cells (Figure 3B). The specificity of SNX9 depletion was confirmed with an siRNA sequence targeting a second region of SNX9 (Figures S3B and S3C).

To definitively establish that SNX9 functions in non-clathrin-dependent endocytosis, we used siRNAs to deplete clathrin heavy chain (CHC) by 90%, under conditions which do not alter SNX9 or actin protein levels (Figure 3B). In contrast to SNX9 depletion, CHC depletion did not significantly alter the level of HRP uptake (Figure 3B; n = 3). In addition, codepletion of CHC and SNX9 did not further reduce HRP uptake over SNX9 depletion alone (Figure 3B; n = 3). Thus, in addition to its known role in clathrin-dependent endocytosis, SNX9 is also required for a second clathrin-independent, constitutive fluid-phase endocytic pathway.

Overexpression of dominant-negative dynamin inhibits both clathrin- and caveolin-mediated endocytosis and induces a clathrin-independent compensatory endocytic pathway (Damke et al., 1995). As previously reported, overexpression of dyn2-K44A did not disrupt fluid-phase internalization of HRP (Figure 3C), indicating that SNX9 depletion and dynamin inhibition differentially effect fluid-phase uptake. Strikingly, SNX9 depletion had no effect on HRP uptake in dyn2-K44A-expressing cells, demonstrating that SNX9 is not required for the dyn2-K44A-induced compensatory endocytic pathway. These data underscore the diversity of endocytic machinery used by mammalian cells.

Since SNX9 colocalizes with actin at multiple sites on the plasma membrane, we examined whether the SNX9-dependent fluid-phase endocytic pathway was also actin dependent. Disruption of F-actin with 1 μM latrunculin A (LatA), a drug that sequesters actin monomers (Coue et al., 1987), resulted in a 30 ± 7% (n = 3, p = 0.008) reduction in HRP uptake (Figure 3D). Importantly, treatment of SNX9-depleted cells with LatA did not further reduce HRP uptake levels (Figure 3D), suggesting that SNX9 functions in a pathway together with F-actin to facilitate fluid-phase endocytosis.

SNX9 Stimulates N-WASP-Mediated Activation of the Arp2/3 Complex and Promotes F-Actin Branching

The spatial and temporal coordination of SNX9, N-WASP, and actin suggests that these proteins may function together at many sites of endocytosis. N-WASP exists in an autoinhibited conformation that can be relieved by interactions with the Rho-family GTPase Cdc42, phosphatidylinositol-4,5-bisphosphate ($PI_{4,5}P_2$), and SH3 domain-containing binding partners (Stradal et al., 2004). Since SNX9 contains an SH3 domain, we examined whether it interacts directly with N-WASP in vitro. As shown in Figure 5B, 6xHis-N-WASP associated with GST-SNX9 but not with GST alone. Therefore, we also examined whether SNX9 could affect the in vitro activities of N-WASP to simulate Arp2/3 complex-mediated F-actin nucleation using a pyrene actin assembly assay. In the absence of either N-WASP or the Arp2/3 complex, SNX9
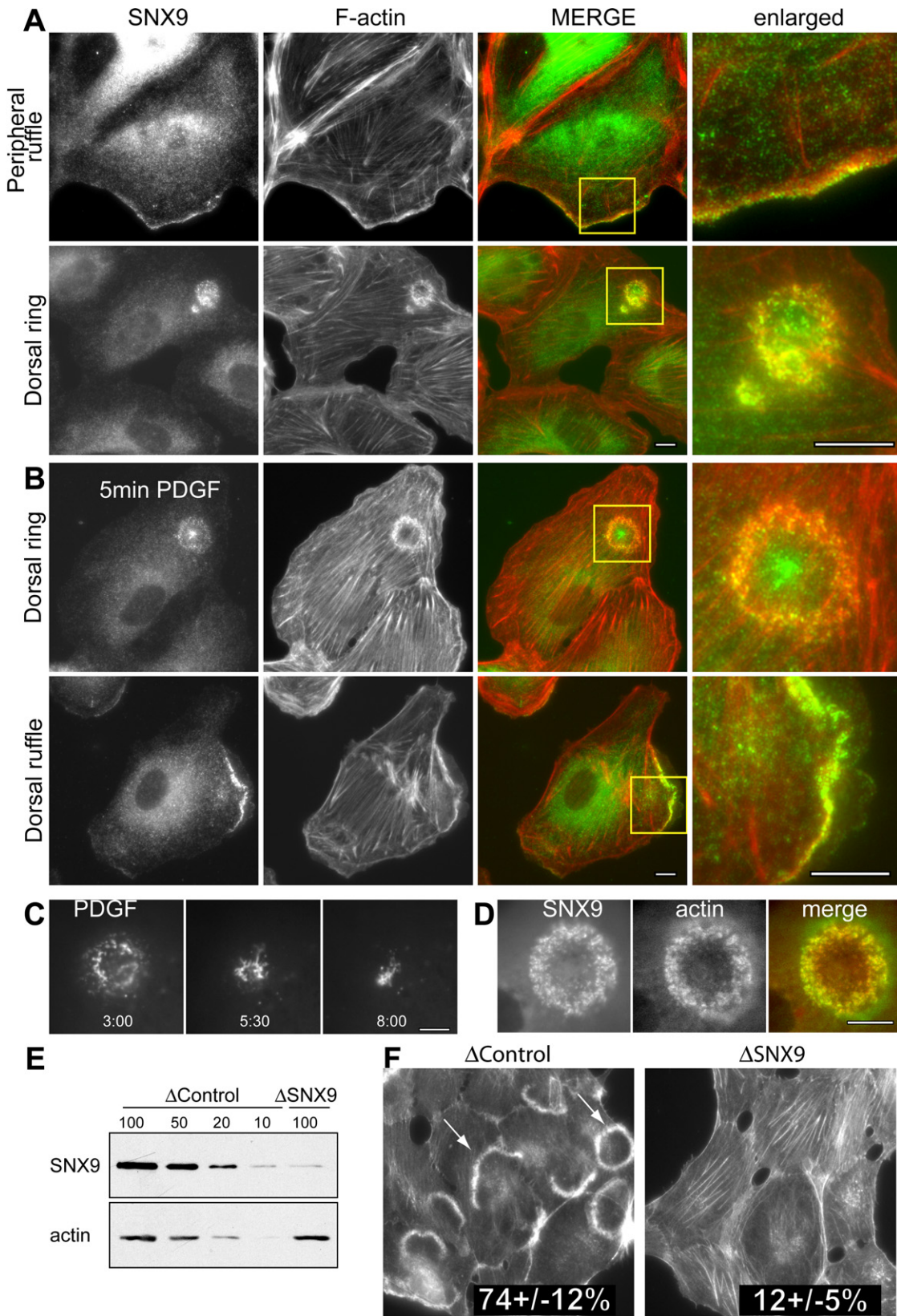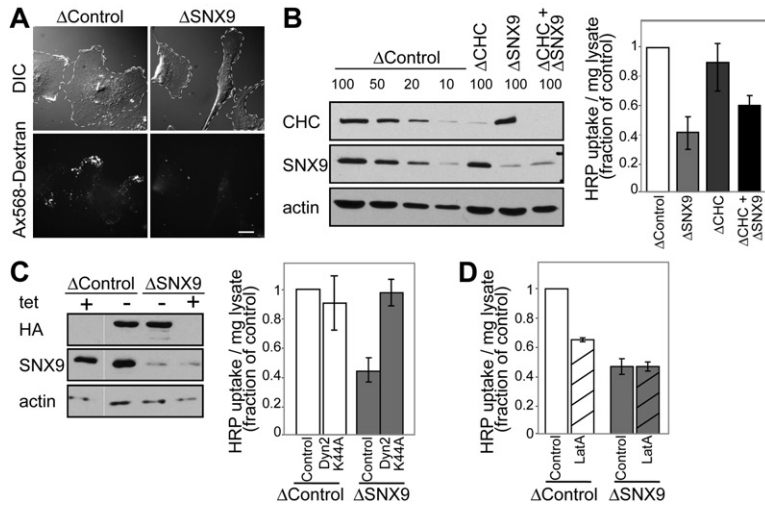
Figure 3. SNX9 Is Required for Clathrin-Independent, F-Actin-Dependent Fluid-Phase Endocytosis

(A) Fluid-phase endocytosis is reduced in SNX9-depleted cells. Shown are DIC (upper, cells are outlined) and fluorescence (lower) images of BSC1 cells treated with SNX9 or control siRNA and incubated for 10 min with 0.25 mg/ml Alexa-568 dextran. See Figure 1E for western blot. Scale bar = 5 μm.

(B) SNX9 is required for clathrin-independent fluid-phase uptake. HRP uptake assays and quantitative western blot (as in Figure 2E) of siRNA-treated lysates from control-, clathrin heavy chain (CHC)-, SNX9-, or CHC and SNX9- depleted BSC1 cells. Blots were probed with antibodies against CHC, SNX9, and actin (as a loading control). The extent of HRP uptake/mg of cell lysate was measured after 8 min incubation in control- (white bar), SNX9- (light gray bar), CHC- (dark gray bar), and SNX9- and CHC-depleted cells (black bar). Results are normalized to controls and shown as mean ± standard deviation, n = 4.

(C) SNX9 is not required for dominant-negative dynamin-induced compensatory fluid-phase uptake. HRP uptake assays and western blots of siRNA-treated lysates from control or SNX9-depleted cells infected with tetracycline-regulable HA-dyn2 K44A-expressing adenoviruses in the presence (+) or absence (−) of tetracycline. Blots were probed with antibodies against HA, SNX9, and actin. The extent of HRP uptake, determined as in Figure 2B, is shown in control (white bars) and SNX9-depleted cells (gray bars).

(D) SNX9 and F-actin function in the same fluid-phase uptake pathway. HRP in control (white bars) and SNX9- depleted cells (gray bars) treated with DMSO (control) or 1 μM LatA (LatA, hatched bars). n = 2.

did not significantly alter F-actin assembly dynamics (Figure 4A). However, in the presence of both N-WASP and Arp2/3, SNX9 stimulated N-WASP nucleation-promoting activity in a dose-dependent manner (Figure 4B; Figure S4). Using a more stringent test, we found that SNX9 also activated ΔEVH1 N-WASP, an N-WASP truncation mutant lacking the WH1/EVH1 domain (ΔEVH1 N-WASP) that exhibits increased autoinhibition (Figure 4C; Figure S4).

The Arp2/3 complex binds to the sides of actin filaments and promotes the growth and nucleation of new filaments to drive the formation of branched, dendritic F-actin arrays in vivo and in vitro (Pollard et al., 2000). Stimulation of Arp2/3-mediated actin nucleation by WASP-family proteins increases the formation of F-actin branches (Amann and Pollard, 2001). To determine whether SNX9 stimulates F-actin nucleation and branching by Arp2/3, we visualized the actin structures formed using TIR-FM of fluorescent actin (Kuhn and Pollard, 2005). In the absence

of other proteins, actin assembled into long, linear filaments (Figure 4D [top panel]; Movie S9). However, consistent with previous work, in the presence of the Arp2/3 complex and ΔEVH1 N-WASP, actin filaments formed dendritic assemblies with many F-actin Y branches (Figure 4D [middle panel]; Movie S9). While SNX9 alone did not alter the morphology of the linear actin structures (data not shown), addition of SNX9 to a mixture of the Arp2/3 complex and ΔEVH1 N-WASP dramatically increased the density of the branches that assembled (Figure 4D [bottom panel]; Movie S9). In total, these results demonstrate that SNX9 binds to and stimulates N-WASP activation of the Arp2/3 complex, yielding highly branched arrays of F-actin.

The SH3 Domain of SNX9 Is Necessary but Not Sufficient for Full N-WASP Activation

To identify the regions of SNX9 required for binding to and activating N-WASP, we generated deletion mutants

Figure 2. SNX9 Is Present in Multiple F-Actin-Rich Structures and Is Required for Dorsal Ruffle and Ring Formation

(A) SNX9 is enriched in peripheral ruffles (top) and dorsal rings (bottom). Epi-fluorescence images of immunofluorescence labeling of endogenous SNX9 (left, green in merge) and phalloidin staining of F-actin (second from left, red in merge) are shown. This is more clearly seen in an enlargement of the yellow boxed area from merged image (right).

(B) Immunofluorescence as in (A) showing that SNX9 is enriched in dorsal ring structures (top) and in dorsal ruffles (bottom) in PDGF-stimulated cells.

(C) mCherry-SNX9 localizes to puncta and tubules in PDGF-induced dorsal rings in time-lapse epi-fluorescence images. Time (min:s) after the addition of PDGF is shown. See Movie S5.

(D) mCherry-SNX9 (left, red in merge) partially colocalizes with EGFP-actin (center, green in merge) in dorsal ring in PDGF-stimulated cell. See Movie S6 and S7.

(E) Quantitative western blots of siRNA-treated lysates from control or SNX9-depleted BSC1 cells using antibodies against SNX9 and actin. Serial dilutions of control lysate (100%–10%) were loaded as indicated.

(F) PDGF-induced dorsal ruffle and ring formation is reduced in SNX9-depleted cells. Shown is phalloidin staining of cells treated with control (left) or SNX9 (right) siRNAs and the corresponding percentage of cells that form dorsal rings or ruffles (mean ± standard deviation, 100–200 cells counted/experiment, n = 3). Scale bars = 5 μm.
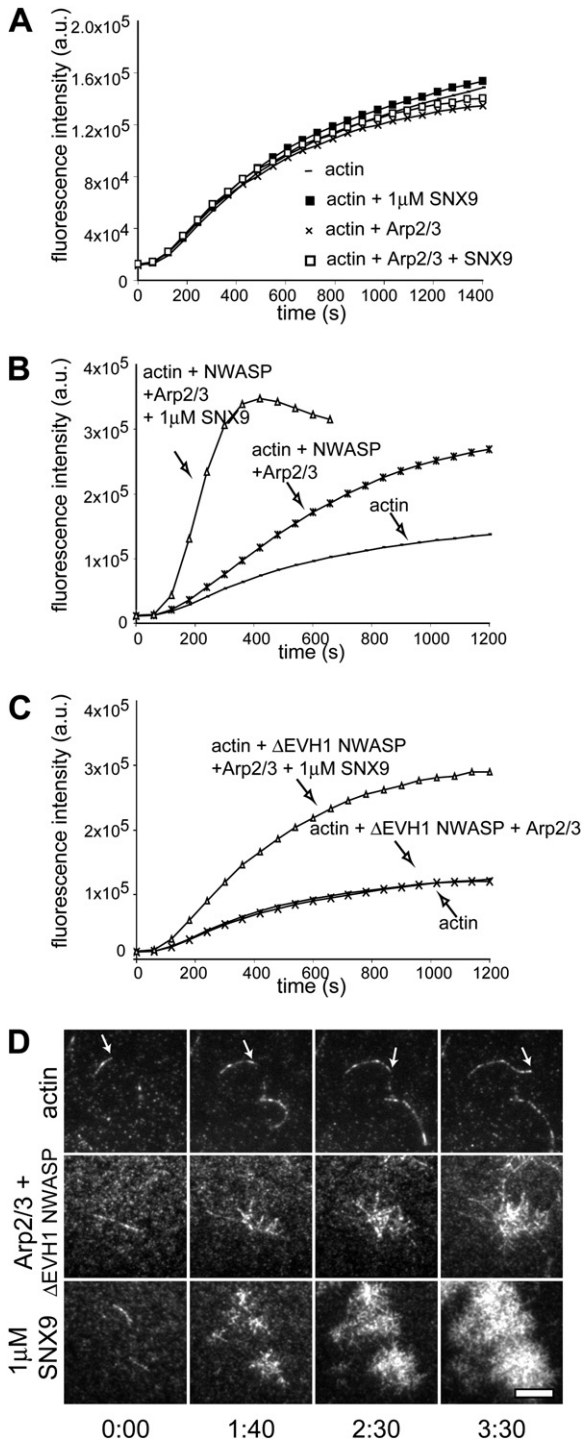
Figure 4. SNX9 Stimulates the Ability of N-WASP to Promote Arp2/3-Complex-Dependent F-Actin Nucleation

(A–C) Pyrene actin assembly assays showing that (A) SNX9 does not significantly affect F-actin kinetics in the absence of N-WASP or Arp2/3 complex. (B) SNX9 activates N-WASP and (C) ΔEVH1 N-WASP. Unless otherwise stated, for all subsequent figures, protein concentrations used in pyrene actin assembly assays are 1.7 μM actin, 15 nM Arp2/3 complex, (B) 30 nM N-WASP, or (C) 100 nM ΔEVH1 N-WASP, and 1 μM SNX9. 1.7 μM actin + 15 nM Arp2/3 complex + 30 nM N-WASP is denoted as double asterisk (**), and 1.7 μM actin +

lacking the SH3 (ΔSH3 SNX9) or PX (ΔPX SNX9) domains, and a fragment of SNX9 containing only the SH3 domain (Figure 5A; Figure S5). SNX9 mutants lacking the BAR domain or mutated to compromise BAR domain activity were insoluble (data not shown), precluding their analysis. SNX9 derivatives containing the SH3 domain (GST-ΔPX SNX9 and GST-SH3) interacted with recombinant N-WASP and ΔEVH1 N-WASP in a GST pull-down assay (Figure 5B; data not shown). In contrast, GST-ΔSH3 SNX9 was unable to bind to either N-WASP derivative, demonstrating that the SH3 domain is both necessary and sufficient for the N-WASP interaction (Figure 5B).

We next tested the relative abilities of the SNX9 derivatives to activate the nucleation-promoting activity of N-WASP. Addition of 1 μM His-ΔPX SNX9, and to a lesser extent GST-SNX9 SH3, to N-WASP or ΔEVH1 NWASP and the Arp2/3 complex increased the rate of F-actin assembly (Figures 5C and 5D; Figure S5B). However, these SNX9 derivatives activated N-WASP less than full-length SNX9, indicating that multiple regions of SNX9 are required for maximal stimulatory activity. In contrast, His-ΔSH3 SNX9 was unable to stimulate N-WASP activity and may exhibit a subtle inhibitory effect on N-WASP activation (Figure 5C). Thus, although the SH3 domain of SNX9 is sufficient for interaction with N-WASP, additional regions of SNX9 are required for full activation of N-WASP.

SNX9 Synergizes with $PI_{4,5}P_2$ to Activate N-WASP

Our in vivo and in vitro data suggest that SNX9 activates N-WASP to trigger Arp2/3-dependent actin assembly at sites of plasma membrane deformation during endocytosis and membrane ruffling. The plasma membrane is enriched in and in part defined by $PI_{4,5}P_2$, which can partially promote N-WASP activity (Rohatgi et al., 1999). SNX9 also interacts directly with phosphatidylinositols through its lipid-binding PX and BAR domains (Lundmark and Carlsson, 2003). Therefore, to determine whether the lipid environment can influence SNX9 activity, we examined if interaction with $PI_{4,5}P_2$-containing liposomes enhanced its ability to stimulate N-WASP. To maximize sensitivity, we tested the effects of $PI_{4,5}P_2$ and SNX9 on the activity of strongly autoinhibited ΔEVH1 N-WASP. Under these assay conditions, addition of either 100 nM SNX9 or 50 μM $PI_{4,5}P_2$-containing liposomes alone did not activate N-WASP/Arp2/3-mediated actin assembly (Figure 6A). However, when SNX9 and 50 μM $PI_{4,5}P_2$ liposomes were added together, we observed a synergistic activation of ΔEVH1 N-WASP and the Arp2/3 complex (Figure 6A). Importantly,

15 nM Arp2/3 complex + 100 nM ΔEVH1 N-WASP is denoted as asterisk (*).

(D) SNX9 stimulates the branching activity of the Arp2/3 complex through N-WASP, as detected by time-lapse TIR-FM of Alexa-488 actin assembly (min:s). Pre-existing filaments can appear by dropping into the evanescent field. The end of an elongating actin filament is marked by an arrow. See Movie S9. 1.1 μM actin (top panels), ± 15 nM Arp2/3 complex and 100 nM ΔEVH1 N-WASP (middle panels), ± 1 μM SNX9 (bottom panels).
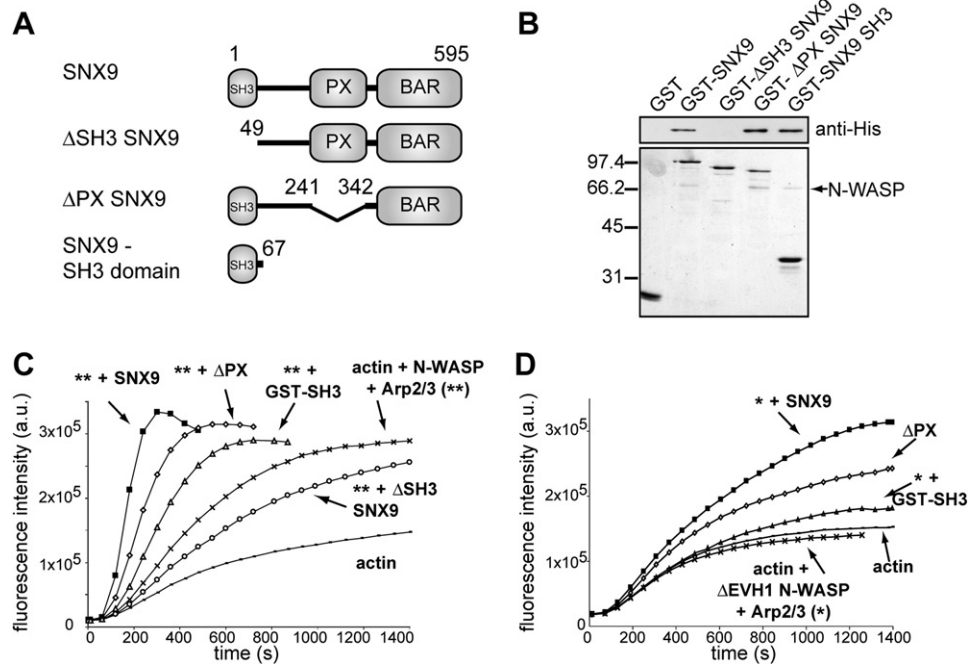
Figure 5. Multiple SNX9 Domains Are Required to Fully Stimulate N-WASP Activity

(A) Schematics of SNX9 and deletion derivatives used in these studies.

(B) The SNX9 SH3 domain is necessary and sufficient to bind to N-WASP. 2 μM GST-SNX9 derivative pull-downs of 1 μM 6xHis-N-WASP analyzed by western blot using anti-Penta His antibodies to detect 6xHis-N-WASP (top) and Coomassie blue staining (bottom).

(C and D) Full-length SNX9 is required for maximal activity. Pyrene actin assembly assays show the relative abilities of 1 μM SNX9 derivatives to activate (C) N-WASP or (D) ΔEVH1 N-WASP.

in the absence of ΔEVH1 N-WASP, addition of SNX9 and 50 μM $PI_{4,5}P_2$ had no effect on the rate of Arp2/3-mediated actin assembly (Figure S6A). Interestingly, this synergistic activity of SNX9 with $PI_{4,5}P_2$ liposomes required their preincubation for 30 min at 25°C prior to addition to the actin assembly mix. Combining 100 nM SNX9 with either 50 μM (Figure 6A) or 100 μM (data not shown) $PI_{4,5}P_2$ liposomes without any prior incubation did not synergistically activate N-WASP. This effect was also dependent on the presence of $PI_{4,5}P_2$, because PC liposomes did not affect actin polymerization (Figures S6B and S6C). The ability of SNX9 to synergize with $PI_{4,5}P_2$ depends on the lipid-binding domains of SNX9 as neither ΔPX SNX9 nor GST-SH3 SNX9 exhibited synergy with $PI_{4,5}P_2$ liposomes (Figure 6B). These results demonstrate that the presence of the lipid-binding and SH3 domains in SNX9 together promote N-WASP- and Arp2/3-dependent F-actin nucleation.

Other BAR/F-BAR and SH3 domain-containing proteins have been identified that associate with N-WASP and therefore have the potential to simultaneously interact with phosphatidylinositols and N-WASP (Dawson et al., 2006). Therefore, we tested whether the activation by $PI_{4,5}P_2$-containing liposomes was specific to SNX9. Similar to SNX9, syndapin II is an F-BAR and SH3 domain-containing protein that associates with N-WASP in cell lysates and has been suggested to regulate F-actin assembly during endocytosis (Kessels and Qualmann,

2002; Qualmann et al., 1999). Immobilized GST-syndapin II was able to pull down recombinant ΔEVH1 N-WASP (Figure 6C), although to a much lower extent than the GST-SH3 domain of SNX9. Consistent with this, syndapin II could also stimulate the activity of ΔEVH1 N-WASP, albeit to a lower extent than SNX9 (Figure 6D). In contrast, syndapin II did not synergistically activate ΔEVH1 N-WASP when preincubated with $PI_{4,5}P_2$ liposomes (Figure 6F), even though it was able to bind to and cosediment with these liposomes (Figure 6E). These results establish specificity with respect to the ability of SNX9 to synergize with $PI_{4,5}P_2$ liposomes.

Oligomeric SNX9 Exhibits Higher Activity Than Dimeric SNX9

The requirement for preincubation to detect $PI_{4,5}P_2$ stimulation of SNX9 suggests that a structural or conformational change may be necessary to mediate this effect. In the course of purifying recombinant SNX9 by gel filtration, we observed two His-SNX9 species, one eluting with a Stokes radius of 6.2–8.0 nm and a more variably present larger species eluting with a Stokes radius of 13.5–16.8 nm. (Figure 7A). Velocity sedimentation analyses indicated S-values of ∼5.6S and between 5.6 and 10.0S for the smaller and larger species, respectively (Figure 7B). Together these hydrodynamic properties indicate that the smaller species corresponds to a dimer of SNX9, while the larger species consists of an oligomer of 5–10 subunits.
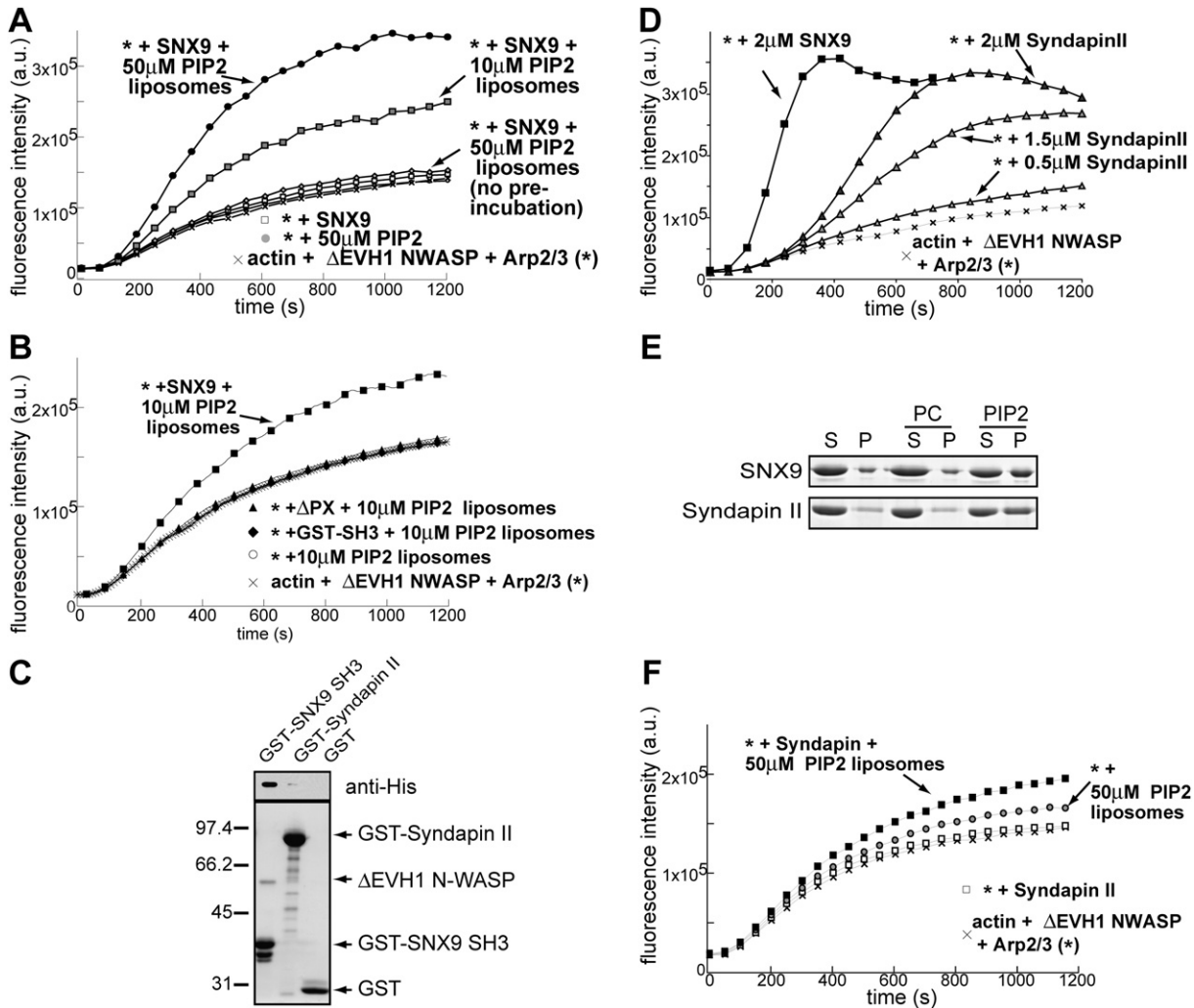
Figure 6. PI$_{4,5}$P$_2$ Liposomes Induce SNX9 Oligomerization and Synergize with SNX9 to Activate ΔEVH1 N-WASP

(A) SNX9 must be preincubated with PI$_{4,5}$P$_2$ liposomes to synergistically activate ΔEVH1 N-WASP. Conditions are similar to those described in Figure 4, with the exception that 100 nM SNX9 was preincubated for 30 min at 25°C with either 50 μM PI$_{4,5}$P$_2$ (black circles) or 10 μM (gray squares) PI$_{4,5}$P$_2$ liposomes. 100 nM SNX9 and 50 μM PI$_{4,5}$P$_2$ liposomes were assayed without preincubation (open diamonds).

(B) SNX9 lipid-binding domains are required for synergy with PI$_{4,5}$P$_2$ liposomes. Addition of 100 nM SNX9 derivatives preincubated for 30 min at 25°C with 10 μM PI$_{4,5}$P$_2$ liposomes does not activate ΔEVH1 N-WASP.

(C) Syndapin II can directly interact with ΔEVH1 N-WASP, shown by GST-SNX9 SH3 or GST-syndapin II pull-downs of ΔEVH1 N-WASP analyzed by western blot using anti-His antibodies to detect 6xHis-ΔEVH1 N-WASP (top) and Coomassie blue staining (bottom).

(D) Dose-dependent activation of ΔEVH1 N-WASP by syndapin II. 2 μM SNX9 is shown for comparison.

(E) Coomassie-stained gel showing that SNX9 and syndapin II interact and cosediment with PI$_{4,5}$P$_2$ liposomes but not PC liposomes.

(F) Syndapin II and PI$_{4,5}$P$_2$ liposome activation of ΔEVH1 N-WASP is additive, not synergistic. 100 nM syndapin II was preincubated as in (B) with 50 μM PI$_{4,5}$P$_2$ liposomes (black squares) before addition to assay.

Strikingly, when assayed in the presence of both ΔEVH1 N-WASP and the Arp2/3 complex, the SNX9 oligomer was significantly more potent than the SNX9 dimer (Figures 4 and 7D). While as little as 30 nM SNX9 oligomer potently stimulated ΔEVH1 NWASP and Arp2/3 complex-mediated F-actin assembly in a dose-dependent manner (Figure 7D; Figure S7), under these conditions 125 nM SNX9 dimer had little effect. Importantly, in control experiments, we found that oligomeric SNX9 (Figure 7C), like dimeric SNX9 (Figure 4A), had no effect on F-actin polymerization

when assayed in the absence of either ΔEVH1 N-WASP or the Arp2/3 complex.

The ability of dimeric SNX9 to stimulate N-WASP activity is potently enhanced by either preincubation with PI$_{4,5}$P$_2$ liposomes or by SNX9 oligomerization. To test for a relationship between these two conditions, we performed nondenaturing polyacrylamide gel electrophoresis in the presence of excess detergent to assess the oligomerization state of SNX9 following preincubation with PI$_{4,5}$P$_2$ liposomes (Figure 7E). In the absence of

liposomes, SNX9 primarily migrated near the bottom of the gel, consistent with its dimeric nature. Incubation of dimeric SNX9 with detergent alone or with PC liposomes, which do not bind to SNX9, did not alter its migration properties in the native gel. In contrast, incubation of SNX9 with $PI_{4,5}P_2$ -containing liposomes significantly slowed the migration of SNX9, suggesting the formation of oligomers (Figure 7E). To determine if association with a lipid membrane is sufficient to induce oligomerization and activation of SNX9, His-SNX9 was incubated with nickel-NTA-containing liposomes (15 mol% Ni-NTA and 85 mol% PC) and examined for its activity level and oligomerization state. In this experiment, untagged ΔEVH1 N-WASP was used so that the His tag did not affect interpretation of results. Although His-SNX9 efficiently pelleted with nickel-NTA-containing liposomes (Figure S7B), this interaction did not induce SNX9 oligomerization (Figure 7E) or enhance ΔEVH1 N-WASP activity (Figure 7F). Taken together, these data suggest that in the presence of $PI_{4,5}P_2$, SNX9 is induced to undergo oligomerization that in turn results in a dramatic increase in the ability of SNX9 to activate N-WASP. These findings suggest a novel mechanism by which SNX9 can couple phosphoinositide signaling to actin assembly and affect plasma membrane remodeling during endocytosis.

DISCUSSION

SNX9 Functions in Coupling Actin Dynamics to Membrane Remodeling in Multiple Modes of Endocytosis

F-actin dynamics play a critical role in remodeling the plasma membrane. However, the mechanism coupling regulation of F-actin assembly to membrane remodeling during endocytosis has remained poorly defined. Using a combination of in vivo and in vitro approaches, we have identified SNX9 as a molecular link that could couple membrane association with de novo F-actin nucleation through modulation of N-WASP activity during multiple modes of endocytosis.

In addition to the previously established requirement for SNX9 in clathrin-mediated endocytosis (Soulet et al., 2005), we now show that SNX9 participates in clathrin-independent, F-actin-dependent constitutive fluid-phase endocytosis. SNX9, N-WASP, and actin assembly are spatially and temporally coordinated at membrane tubules containing GPI-APs, and the dynamics of actin assembly appear to locally correlate with tubule motion. This suggests the involvement of these proteins in the recently identified GEEC pathway thought to be a major route for the uptake of GPI-APs and fluid (Kirkham et al., 2005; Mayor and Riezman, 2004). SNX9, N-WASP, and actin dynamics are also spatio-temporally coordinated with the motion of PDGF-induced dorsal ruffles and rings, suggesting that ruffle motion is powered by SNX9-mediated actin assembly (Buccione et al., 2004; Legg et al., 2007; this study). SNX9, N-WASP, and actin are also recruited to clathrin-coated pits on the plasma membrane at late stages of clathrin-coated vesicle formation (Merri-

field et al., 2002, 2004; Soulet et al., 2005; Yarar et al., 2005). As siRNA-mediated depletion of SNX9 inhibits fluid-phase endocytosis, membrane ruffling, and clathrin-mediated endocytosis (Soulet et al., 2005; this study), we propose that the local recruitment of SNX9 to membrane sites of endocytosis results in N-WASP activation to promote the local assembly of a dendritic actin network through activation of the Arp2/3 complex. The force generated by network assembly at the membrane then drives the local membrane deformations required for specific aspects of these different modes of endocytosis.

Although SNX9 is a major dynamin-binding partner (Soulet et al., 2005), SNX9 depletion inhibits fluid-phase uptake, while dominant interference of dynamin does not. Because dominant-negative dynamin expression induces a dynamin- and clathrin-independent compensatory endocytic pathway that is also independent of SNX9, we cannot conclude that SNX9 functions independently of dynamin during fluid-phase uptake. Nevertheless, induction of a compensatory pathway upon inhibition of endocytosis by dynamin, but not after depletion of either SNX9 or clathrin, is an unexpected observation that underscores the diversity and versatility of endocytic pathways in mammalian cells. Together, our results demonstrate a novel role for SNX9 during multiple modes of endocytosis.

Oligomerization and $PI_{4,5}P_2$-Containing Liposomes Enhance SNX9 Activity

Recombinant SNX9 exists predominantly as a dimer. However, we were also able to isolate a small proportion of SNX9 as a higher-order oligomer and show that this oligomeric species was dramatically more active in stimulating N-WASP- and Arp2/3-dependent actin assembly. Although the mechanism of oligomerization in E. coli is unclear, it may reflect either the high concentration of recombinant protein in the bacterium-promoted His-SNX9 assembly or the association of recombinant SNX9 with bacterial proteins, lipids, or polyphosphates. Regardless, this fortuitous observation provided mechanistic insight into SNX9 activation. Interestingly, other BAR- and F-BAR-containing proteins, including FBP17, CIP4, and syndapin II, have also been suggested to oligomerize (Dawson et al., 2006). However, no activity has been previously connected with this oligomerization.

SNX9 oligomerization is promoted by $PI_{4,5}P_2$ binding. $PI_{4,5}P_2$-induced SNX9 assembly may result from an increased local concentration of SNX9 on the 2D surface of the liposome and/or from a conformational change that facilitates oligomerization. Importantly, forced interaction of His-SNX9 with nickel-NTA-containing liposomes failed to promote SNX9 assembly, suggesting that a phosphoinositide interaction is required. Although we cannot exclude the possibility that incubation of SNX9 with liposomes might modify the lipid environment (i.e., by clustering the $PI_{4,5}P_2$), we suggest that the increased activity observed upon liposome association is a result of SNX9 oligomerization and may partly result from N-WASP clustering. Previous in vivo studies have shown that artificially
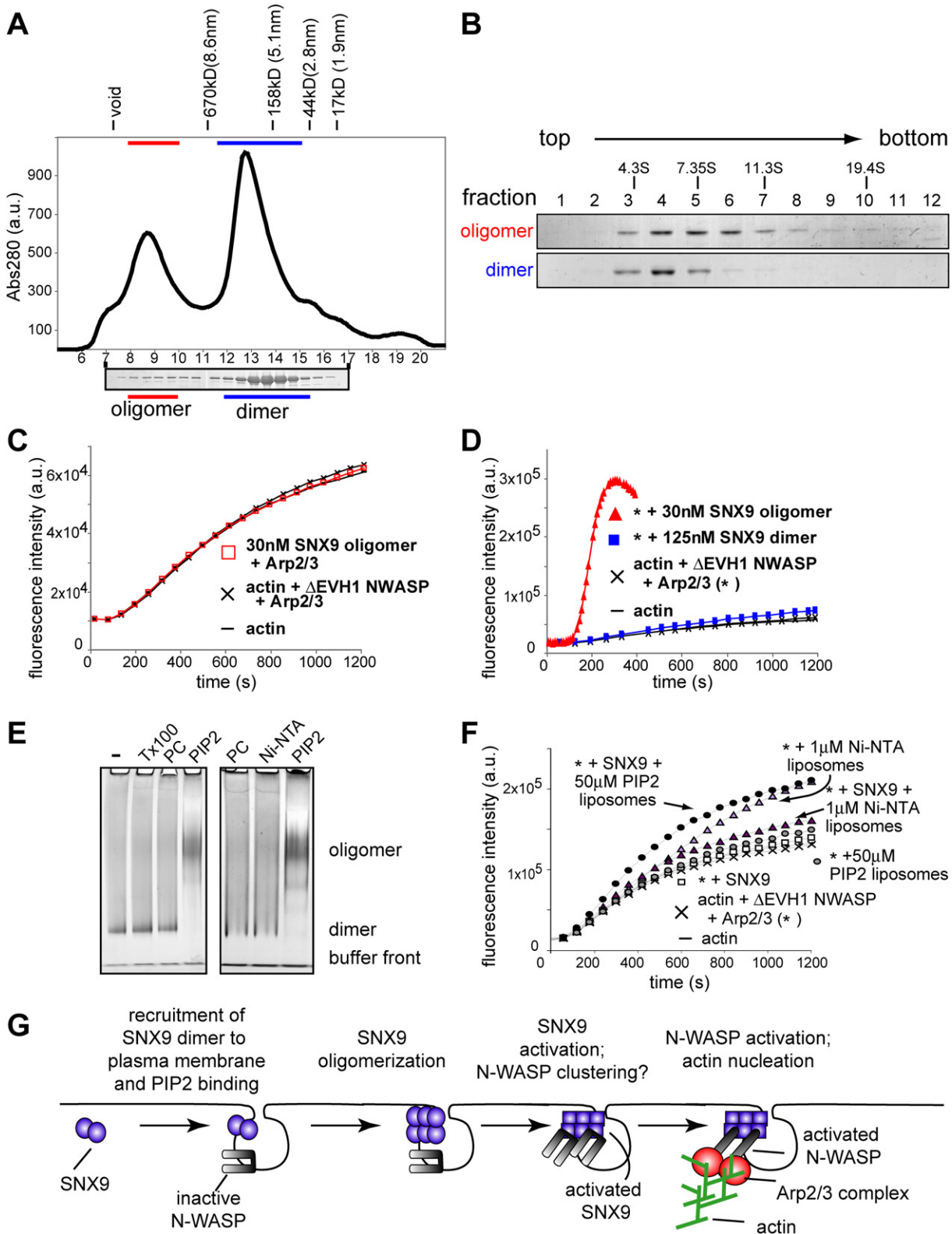
Figure 7. SNX9 Oligomer Is a More Potent N-WASP Activator Than SNX9 Dimer

(A) Gel filtration of 6xHis-SNX9 and corresponding Coomassie blue-stained gel of peak fractions (7–17) reveals two main SNX9 species. Gel filtration standards (molecular weights and Stokes radii) are indicated above graph. Oligomeric and dimeric fractions used in experiments are marked/underscored by the red and blue line, respectively.

induced clustering of WASP (a hematopoetic-specific WASP-family protein, structurally similar to N-WASP) on the plasma membrane resulted in F-actin polymerization and the formation of membrane protrusions (Castellano et al., 1999). Alternatively, or in addition, the increase in SNX9's stimulation of N-WASP could be caused by a conformational change within SNX9 that releases an autoinhibitory, intramolecular interaction (Worby et al., 2001). Thus, interaction with PI$_{4,5}$P$_2$ liposomes could modulate inter- and intramolecular interactions that regulate both SNX9 oligomerization and autoinhibition.

The finding that SNX9 has broad phospholipid-binding specificity (Lundmark and Carlsson, 2003) suggests that other phosphatidylinositols may also regulate SNX9 activity. Indeed, it was recently shown that T cell/CD28 stimulation induces the formation of a multimeric signaling complex containing SNX9, WASP, and p85, the regulatory subunit of PI-3 kinase, at sites of clathrin-mediated endocytosis (Badour et al., 2007). These data support a more general role for SNX9 in coupling phosphoinositide signaling to actin dynamics during endocytosis.

A Model for SNX9 Regulation of Actin Assembly at the Plasma Membrane

Together, our in vivo and in vitro data suggest a mechanism by which SNX9 spatially and temporally coordinates F-actin nucleation and membrane remodeling during endocytosis (Figure 7G). We propose that the discrete accumulation of SNX9 observed at the tips of GFP-GPI tubules and the dynamic association of SNX9 with membrane ruffles reflects a PI$_{4,5}$P$_2$-induced critical, activating conformational change that is followed by SNX9 self-assembly. Interestingly, we have previously observed a similar "burst" of SNX9 at clathrin-coated pits (Soulet et al., 2005). Since we find that localization of SNX9 and N-WASP is spatially and temporally coordinated, we propose that the locally activated SNX9 both clusters and stimulates N-WASP to promote Arp2/3-mediated actin filament nucleation. Filament elongation of a highly branched actin network would provide the force required for membrane reshaping during vesicle invagination and/or scission and for the extension of dorsal ruffles. Consistent with this, actin also appeared brighter at the edges of dynamic GFP-GPI tubules and colocalized with SNX9 in PDGF-induced ruffles. Further work will be necessary to test aspects of this model and to define the mechanisms

of SNX9 regulation in coordinating actin assembly with membrane remodeling during endocytosis.

EXPERIMENTAL PROCEDURES

Cell Culture
BSC1 cells (ATCC) or BSC1 CLC-EGFP-expressing cells (kindly provided by T. Kirchhausen) were grown at 37°C, 5% CO$_2$ and maintained in DMEM containing 10% FBS (Gemini).

Microscopy
For indirect immunofluorescence, BSC1 cells were plated onto coverslips and fixed with 4% paraformaldehyde (PFA). Cells were permeabilized in PBS containing 0.1% saponin and 2% BSA and incubated with affinity-purified, polyclonal anti-SNX9 antibodies (5 μg/ml) (Soulet et al., 2005), Alexa-488-conjugated anti-rabbit secondary antibodies (Invitrogen), and/or Alexa-568 phalloidin (Invitrogen). For PDGF stimulation, cells were starved for 24 hr in DMEM containing 0.2% FCS and stimulated for 5 min with 30 ng/ml PDGF-BB (Calbiochem) before fixation and staining. Images were obtained as previously described (Wittmann et al., 2003).

To image mCherry-SNX9, EGFP-NWASP, GFP-GPI, or mCherry-actin, plasmids were transfected into BSC1 cells with Effectene (QIAGEN) and imaged 16–20 hr posttransfection. Near-simultaneous, total internal reflection fluorescence microscopy (TIR-FM) images of mCherry- or EGFP-fusion proteins were collected at 2.5–5 s intervals using an Orca II/ERG CCD camera in 14-bit mode (Adams et al., 2004; Soulet et al., 2005). Images presented in movie sequences and kymographs were subjected to a Gaussian filter (kernel 3) in Metamorph software (Molecular Devices) for presentation. Pairs of images were acquired at 5 s intervals using epi-fluorescence mode and imaging conditions as previously described (Adams et al., 2004; Yarar et al., 2005). For colocalization analyses, TIR-FM images were contrast enhanced, pseudo-colored, and merged using Metamorph to identify SNX9 foci that were positive for EGFP-N-WASP.

siRNA Treatment
8.0×10^4 cells were plated into 35 mm dishes and allowed to grow for 24 hr. 80 nM siRNA (SNX9 siRNA #1:sense UAAGCACUUUGACUGGUUAUU; control nontargeting siRNA #1 [Dharmacon]; CHC oligos: sense AAGCUGGGAAAACUCUUCAGAUU [Motley et al., 2003]) were introduced into cells using HiPerFect (QIAGEN) according to the manufacturer's instructions. After 24 hr incubation, cells were plated on 35 mm dishes, retransfected with siRNAs, and assayed 24 hr later for SNX9/CHC depletion by western blotting and for HRP/dextran uptake. BSC1 CLC-GFP cells were used to determine the effect of SNX9 depletion on dorsal ruffle/ring formation.

Endocytosis Assays
HRP uptake assays were performed as previously described (Schlunck et al., 2004). For LatA treatment, cells grown in 35 mm dishes were pretreated with 1 μM LatA (solubilized in DMSO) (Sigma)

(B) Velocity sedimentation profile of SNX9 oligomer (top panel) and dimer (bottom panel). S-values of standards are shown above gels.

(C and D) (C) The SNX9 oligomer has no effect on F-actin assembly kinetics in the absence of N-WASP (D) but more potently activates ΔEVH1 N-WASP than the SNX9 dimer.

(E) PI$_{4,5}$P$_2$-containing liposomes induce SNX9 oligomerization (left gel), but nickel-NTA liposomes do not (right gel). Gels shows 2 μM SNX9 dimer alone (–) or after incubation without (TX-100) or with 200 μM PC liposomes, PI$_{4,5}$P$_2$ liposomes, or nickel-NTA liposomes, as indicated. After incubation, SNX9/liposome mixtures were solubilized with TX-100 and subjected to native gel electrophoresis.

(F) 6xHis-SNX9 and nickel-NTA liposomes do not synergistically activate ΔEVH1 N-WASP. 50 μM PI$_{4,5}$P$_2$ liposomes were incubated either alone (gray circles) or with 100 nM SNX9 (black circles). 1 μM nickel-NTA liposomes were incubated either alone (light purple triangles) or with 100 nM SNX9 (dark purple triangles).

(G) Model of proposed mechanism by which SNX9 couples lipid binding to activation of N-WASP and F-actin nucleation to drive membrane shape changes. SNX9 is shown as a blue circle which self associates upon lipid binding and undergoes a conformational change (blue squares). This results in a more active form of SNX9 that enhances the ability of N-WASP to stimulate the Arp2/3 complex.

or DMSO for 25 min at 37°C and then incubated with HRP in the continued presence of 1 µM LatA or DMSO for the duration of internalization. For dyn2-K44A overexpression, cells grown in 35 mm dishes were transfected with SNX9 or control siRNAs as described above and infected with HA-dyn2 K44A (under control of tetracycline regulatable promoter, tet-off) and tTA transactivator (tTA) adenoviruses in the absence or presence of 1 µg/ml tetracycline. After ~18 hr, cells were assayed for HRP uptake and HA-dyn2 K44A expression by western blotting (anti-HA, 12CA5). Three independent experiments were performed in duplicate, averaged, and normalized to the quantity of HRP internalized in control cells.

For dextran uptake, cells were grown on coverslips and incubated in the presence of 10 kD Alexa-568 fixable dextran (Invitrogen), fixed with 4% PFA, mounted on a coverslip, and imaged with a 40X Fluar, 1.3NA objective (Zeiss) on an upright Zeiss Axiophot epi-fluorescence microscope. Images were collected using an AxioCam HRm digital camera (Zeiss).

Protein Expression and Purification

Recombinant human Arp2/3 complex (Goley et al., 2004), rabbit skeletal muscle actin (Spudich and Watt, 1971), and pyrene-labeled actin (Kouyama and Mihashi, 1981) were prepared as described previously. Rabbit muscle myosin II was provided by Ron Milligan (TSRI). GST- and His-tagged SNX9 derivatives and His-ΔEVH1 N-WASP (aa138–501) were expressed in BL21-DE3 *E. coli*, and cell lysates were subjected to affinity purification using glutathione-Sepharose 4B (Amersham Bioscience) for GST-fusion proteins or Ni-NTA agarose (QIAGEN) for His-tagged proteins according to the manufacturer's instructions. Except for GST-syndapin II, all peak fractions were further purified over a Superose 6 10/300 gel filtration column into control buffer (20 mM HEPES [pH 7.4], 100 mM KCl, 1 mM EDTA, 1 mM EGTA, 2 mM MgCl$_2$, 10% glycerol, and 0.5 mM DTT). Untagged syndapin II was cleaved from GST-syndapin II with PreScission protease (GE Healthcare) and purified by gel filtration. Bovine 6xHis-N-WASP was expressed in Tn5 cells using the baculovirus expression system. Thawed cell pellets were resuspended in 50 mM NaPhosphate (pH 8.0), 400 mM KCl, centrifuged, and purified as above, except that the control buffer contained 300 mM KCl.

Actin Assembly Assays

Pyrene actin assembly assays were performed as previously described (Cooper et al., 1983). Unless otherwise stated, pyrene assays were in the presence of the dimeric SNX9 species. All pyrene curves shown are representative of at least duplicate experiments.

Microscopy-based actin polymerization assays were based on previous studies (Kovar et al., 2006; Kuhn and Pollard, 2005). NEM-treated rabbit muscle myosin was coated on acid-washed glass coverslips and mounted on a slide with two strips of double-sided tape spaced ~0.5 cm apart. Actin assembly was initiated and then transferred to the slide chamber. The coverslip was sealed and immediately imaged by TIR-FM with 100–300 ms exposures, 5 s intervals using the microscope system described in Adams et al. (2004). This microscopy-based assay allows the detection and analysis of those F-actin structures captured on the coverslip and cannot be used to analyze bulk kinetics of the entire population of F-actin.

Liposome Preparation/Binding

Liposomes (100 mol% PC; 15 mol% PI$_{4,5}$P$_2$ + 85 mol% PC; 15 mol% nickel NTA (DOGS) + 85 mol% PC [Avanti]) were prepared as previously described (Soulet et al., 2005).

For liposome-binding experiments, 2 µM protein was incubated with 400 µM liposomes for 45 min in liposome buffer (50 mM HEPES, 100 mM NaCl, 0.5 mM DTT) and centrifuged for 20 min at 20,000 g. The supernatant was removed and the pellet resuspended in an equal buffer volume. Equal volumes of supernatant and pellet samples were analyzed by SDS-PAGE.

To observe liposome-induced SNX9 oligomerization, 2.0 µM SNX9 was incubated with 200 µM liposomes (400 nm) or in liposome buffer

alone for 30 min at room temperature. Samples were treated with 0.7% Triton X-100 (11.9 mM) for 4 min and analyzed by 3%–8% Tris-Acetate Native electrophoresis (Invitrogen).

Sucrose Gradient

150 µl of 6xHis-SNX9 was run on a 2 ml 5%–20% sucrose gradient in control buffer at 50 k rpm for 8 hr at 4°C. 150 µl fractions were taken from the top of the tube and analyzed by SDS-PAGE. Sedimentation was compared to standards: BSA (4.3 S), aldolase (7.35 S), catalase (11.3 S), and thyroglobulin (19.4 S).

Supplemental Data

Supplemental Data include nine movies and seven figures and can be found with this article online at http://www.developmentalcell.org/cgi/content/full/13/1/43/DC1/.

REFERENCES

Adams, M.C., Matov, A., Yarar, D., Gupton, S.L., Danuser, G., and Waterman-Storer, C.M. (2004). Signal analysis of total internal reflection fluorescent speckle microscopy (TIR-FSM) and wide-field epi-fluorescence FSM of the actin cytoskeleton and focal adhesions in living cells. J. Microsc. *216*, 138–152.

Amann, K.J., and Pollard, T.D. (2001). Direct real-time observation of actin filament branching mediated by Arp2/3 complex using total internal reflection fluorescence microscopy. Proc. Natl. Acad. Sci. USA *98*, 15009–15013.

Badour, K., McGavin, M.K., Zhang, J., Freeman, S., Vieira, C., Filipp, D., Julius, M., Mills, G.B., and Siminovitch, K.A. (2007). Interaction of the Wiskott-Aldrich syndrome protein with sorting nexin 9 is required for CD28 endocytosis and cosignaling in T cells. Proc. Natl. Acad. Sci. USA *104*, 1593–1598.

Buccione, R., Orth, J.D., and McNiven, M.A. (2004). Foot and mouth: podosomes, invadopodia and circular dorsal ruffles. Nat. Rev. Mol. Cell Biol. *5*, 647–657.

Castellano, F., Montcourrier, P., Guillemot, J.C., Gouin, E., Machesky, L., Cossart, P., and Chavrier, P. (1999). Inducible recruitment of Cdc42 or WASP to a cell-surface receptor triggers actin polymerization and filopodium formation. Curr. Biol. *9*, 351–360.

Conner, S.D., and Schmid, S.L. (2003). Regulated portals of entry into the cell. Nature *422*, 37–44.

Cooper, J.A., Walker, S.B., and Pollard, T.D. (1983). Pyrene actin: documentation of the validity of a sensitive assay for actin polymerization. J. Muscle Res. Cell Motil. *4*, 253–262.

Coue, M., Brenner, S.L., Spector, I., and Korn, E.D. (1987). Inhibition of actin polymerization by latrunculin A. FEBS Lett. *213*, 316–318.

Damke, H., Baba, T., van der Bliek, A.M., and Schmid, S.L. (1995). Clathrin-independent pinocytosis is induced in cells overexpressing a temperature-sensitive mutant of dynamin. J. Cell Biol. 131, 69–80.

Dawson, J.C., Legg, J.A., and Machesky, L.M. (2006). Bar domain proteins: a role in tubulation, scission and actin assembly in clathrin-mediated endocytosis. Trends Cell Biol. 16, 493–498.

Engqvist-Goldstein, A.E., Kessels, M.M., Chopra, V.S., Hayden, M.R., and Drubin, D.G. (1999). An actin-binding protein of the Sla2/Huntingtin interacting protein 1 family is a novel component of clathrin-coated pits and vesicles. J. Cell Biol. 147, 1503–1518.

Goley, E.D., Rodenbusch, S.E., Martin, A.C., and Welch, M.D. (2004). Critical conformational changes in the Arp2/3 complex are induced by nucleotide and nucleation promoting factor. Mol. Cell 16, 269–279.

Guha, A., Sriram, V., Krishnan, K.S., and Mayor, S. (2003). Shibire mutations reveal distinct dynamin-independent and -dependent endocytic pathways in primary cultures of Drosophila hemocytes. J. Cell Sci. 116, 3373–3386.

Ho, H.Y., Rohatgi, R., Lebensohn, A.M., Le, M., Li, J., Gygi, S.P., and Kirschner, M.W. (2004). Toca-1 mediates Cdc42-dependent actin nucleation by activating the N-WASP-WIP complex. Cell 118, 203–216.

Itoh, T., Erdmann, K.S., Roux, A., Habermann, B., Werner, H., and De Camilli, P. (2005). Dynamin and the actin cytoskeleton cooperatively regulate plasma membrane invagination by BAR and F-BAR proteins. Dev. Cell 9, 791–804.

Kaksonen, M., Toret, C.P., and Drubin, D.G. (2006). Harnessing actin dynamics for clathrin-mediated endocytosis. Nat. Rev. Mol. Cell Biol. 7, 404–414.

Kessels, M.M., and Qualmann, B. (2002). Syndapins integrate N-WASP in receptor-mediated endocytosis. EMBO J. 21, 6083–6094.

Kirkham, M., Fujita, A., Chadda, R., Nixon, S.J., Kurzchalia, T.V., Sharma, D.K., Pagano, R.E., Hancock, J.F., Mayor, S., and Parton, R.G. (2005). Ultrastructural identification of uncoated caveolin-independent early endocytic vehicles. J. Cell Biol. 168, 465–476.

Kirkham, M., and Parton, R.G. (2005). Clathrin-independent endocytosis: new insights into caveolae and non-caveolar lipid raft carriers. Biochim. Biophys. Acta 1745, 273–286.

Kouyama, T., and Mihashi, K. (1981). Fluorimetry study of N-(1-pyrenyl)-iodoacetamide-labelled F-actin. Local structural change of actin protomer both on polymerization and on binding of heavy meromyosin. Eur. J. Biochem. 114, 33–38.

Kovar, D.R., Harris, E.S., Mahaffy, R., Higgs, H.N., and Pollard, T.D. (2006). Control of the assembly of ATP- and ADP-actin by formins and profilin. Cell 124, 423–435.

Kuhn, J.R., and Pollard, T.D. (2005). Real-time measurements of actin filament polymerization by total internal reflection fluorescence microscopy. Biophys. J. 88, 1387–1402.

Lamaze, C., Dujeancourt, A., Baba, T., Lo, C.G., Benmerah, A., and Dautry-Varsat, A. (2001). Interleukin 2 receptors and detergent-resistant membrane domains define a clathrin-independent endocytic pathway. Mol. Cell 7, 661–671.

Legg, J.A., Bompard, G., Dawson, J., Morris, H.L., Andrew, N., Cooper, L., Johnston, S.A., Tramountanis, G., and Machesky, L.M. (2007). N-wasp involvement in dorsal ruffle formation in mouse embryonic fibroblasts. Mol. Biol. Cell 18, 678–687.

Lundmark, R., and Carlsson, S.R. (2003). Sorting nexin 9 participates in clathrin-mediated endocytosis through interactions with the core components. J. Biol. Chem. 278, 46772–46781.

Lundmark, R., and Carlsson, S.R. (2004). Regulated membrane recruitment of dynamin-2 mediated by sorting nexin 9. J. Biol. Chem. 279, 42694–42702.

Mayor, S., and Riezman, H. (2004). Sorting GPI-anchored proteins. Nat. Rev. Mol. Cell Biol. 5, 110–120.

Merrifield, C.J., Feldman, M.E., Wan, L., and Almers, W. (2002). Imaging actin and dynamin recruitment during invagination of single clathrin-coated pits. Nat. Cell Biol. 4, 691–698.

Merrifield, C.J., Perrais, D., and Zenisek, D. (2005). Coupling between clathrin-coated-pit invagination, cortactin recruitment, and membrane scission observed in live cells. Cell 121, 593–606.

Merrifield, C.J., Qualmann, B., Kessels, M.M., and Almers, W. (2004). Neural Wiskott Aldrich Syndrome Protein (N-WASP) and the Arp2/3 complex are recruited to sites of clathrin-mediated endocytosis in cultured fibroblasts. Eur. J. Cell Biol. 83, 13–18.

Mettlen, M., Platek, A., Van Der Smissen, P., Carpentier, S., Amyere, M., Lanzetti, L., de Diesbach, P., Tyteca, D., and Courtoy, P.J. (2006). Src triggers circular ruffling and macropinocytosis at the apical surface of polarized MDCK cells. Traffic 7, 589–603.

Motley, A., Bright, N.A., Seaman, M.N., and Robinson, M.S. (2003). Clathrin-mediated endocytosis in AP-2-depleted cells. J. Cell Biol. 162, 909–918.

Pelkmans, L., Puntener, D., and Helenius, A. (2002). Local actin polymerization and dynamin recruitment in SV40-induced internalization of caveolae. Science 296, 535–539.

Peter, B.J., Kent, H.M., Mills, I.G., Vallis, Y., Butler, P.J., Evans, P.R., and McMahon, H.T. (2004). BAR domains as sensors of membrane curvature: the amphiphysin BAR structure. Science 303, 495–499.

Pollard, T.D., Blanchoin, L., and Mullins, R.D. (2000). Molecular mechanisms controlling actin filament dynamics in nonmuscle cells. Annu. Rev. Biophys. Biomol. Struct. 29, 545–576.

Qualmann, B., Roos, J., DiGregorio, P.J., and Kelly, R.B. (1999). Syndapin I, a synaptic dynamin-binding protein that associates with the neural Wiskott-Aldrich syndrome protein. Mol. Biol. Cell 10, 501–513.

Rohatgi, R., Ma, L., Miki, H., Lopez, M., Kirchhausen, T., Takenawa, T., and Kirschner, M.W. (1999). The interaction between N-WASP and the Arp2/3 complex links Cdc42-dependent signals to actin assembly. Cell 97, 221–231.

Sabharanjak, S., Sharma, P., Parton, R.G., and Mayor, S. (2002). GPI-anchored proteins are delivered to recycling endosomes via a distinct cdc42-regulated, clathrin-independent pinocytic pathway. Dev. Cell 2, 411–423.

Schlunck, G., Damke, H., Kiosses, W.B., Rusk, N., Symons, M.H., Waterman-Storer, C.M., Schmid, S.L., and Schwartz, M.A. (2004). Modulation of Rac localization and function by dynamin. Mol. Biol. Cell 15, 256–267.

Seet, L.F., and Hong, W. (2006). The Phox (PX) domain proteins and membrane traffic. Biochim. Biophys. Acta 1761, 878–896.

Soulet, F., Yarar, D., Leonard, M., and Schmid, S.L. (2005). SNX9 regulates dynamin assembly and is required for efficient clathrin-mediated endocytosis. Mol. Biol. Cell 16, 2058–2067.

Spudich, J.A., and Watt, S. (1971). The regulation of rabbit skeletal muscle contraction. I. Biochemical studies of the interaction of the tropomyosin-troponin complex with actin and the proteolytic fragments of myosin. J. Biol. Chem. 246, 4866–4871.

Stradal, T.E., Rottner, K., Disanza, A., Confalonieri, S., Innocenti, M., and Scita, G. (2004). Regulation of actin dynamics by WASP and WAVE family proteins. Trends Cell Biol. 14, 303–311.

Suetsugu, S., Yamazaki, D., Kurisu, S., and Takenawa, T. (2003). Differential roles of WAVE1 and WAVE2 in dorsal and peripheral ruffle formation for fibroblast cell migration. Dev. Cell 5, 595–609.

Swanson, J.A., and Watts, C. (1995). Macropinocytosis. Trends Cell Biol. 5, 424–428.

Tsujita, K., Suetsugu, S., Sasaki, N., Furutani, M., Oikawa, T., and Takenawa, T. (2006). Coordination between the actin cytoskeleton and membrane deformation by a novel membrane tubulation domain of PCH proteins is involved in endocytosis. J. Cell Biol. 172, 269–279.

Wittmann, T., Bokoch, G.M., and Waterman-Storer, C.M. (2003). Regulation of leading edge microtubule and actin dynamics downstream of Rac1. J. Cell Biol. *161*, 845–851.

Worby, C.A., Simonson-Leff, N., Clemens, J.C., Kruger, R.P., Muda, M., and Dixon, J.E. (2001). The sorting nexin, DSH3PX1, connects the axonal guidance receptor, Dscam, to the actin cytoskeleton. J. Biol. Chem. *276*, 41782–41789.

Yarar, D., Waterman-Storer, C.M., and Schmid, S.L. (2005). A dynamic actin cytoskeleton functions at multiple stages of clathrin-mediated endocytosis. Mol. Biol. Cell *16*, 964–975.